NON-CESIATED SOLID STATE ELECTRON EMITTERS (COLD CATHODES) & THEIR APPLICATIONS IN VACUUM MICROELECTRONICS

FINAL PROGRESS REPORT

Professor Umesh K. Mishra
Robert D. Underwood

May 31, 1999

U.S. ARMY RESEARCH OFFICE

DAAH04-95-1-0157

UNIVERSITY OF CALIFORNIA, SANTA BARBARA
Department of Electrical & Computer Engineering

APPROVED FOR PUBLIC RELEASE;

DISTRIBUTION UNLIMITED.

REPORT DOCUMENTATION PAGE

Form Approved
OMB No. 0704-0188

1. AGENCY USE ONLY *(Leave Blank)*	2. REPORT DATE	3. REPORT TYPE AND DATES COVERED
	31 May 1999	Final Progress

4. TITLE AND SUBTITLE
Non-Cesiated Solid State Electron Emitters (Cold Cathodes) & Their Applications in Vacuum Microelectronics

5. FUNDING NUMBERS
DAAH04-95-1-0157

6. AUTHORS
Prof. Umesh K. Mishra
Robert D. Underwood

7. PERFORMING ORGANIZATION NAME(S) AND ADDRESS(ES)
Department of Electrical & Computer Engineering
University of California, Santa Barbara
Santa Barbara, CA 93106

8. PERFORMING ORGANIZATION REPORT NUMBER

9. SPONSORING / MONITORING AGENCY NAME(S) AND ADDRESS(ES)
U.S. Army Research Office
P.O. Box 12211
Research Triangle Park, NC 27709-2211

10. SPONSORING / MONITORING AGENCY REPORT NUMBER
ARO 33799.7-PH

11. SUPPLEMENTARY NOTES
The views, opinions and/or findings contained in this report are those of the author(s) and should not be construed as an official Department of the Army position, policy or decision, unless so designated by other documentation.

12a. DISTRIBUTION / AVAILABILITY STATEMENT
Approved for public release; distribution unlimited.

12b. DISTRIBUTION CODE

13. ABSTRACT *(Maximum 200 words)*

Stable, non-cesiated cold cathodes hold much promise for high power and high efficiency vacuum electronics. Cesium is typically used to lower the surface barrier to electron emission, but cesium presents problems with reliability and lifetime. GaN-based cold cathodes have the advantage of having a low surface barrier and a stable surface, both of which are beneficial for cold cathode electron emission. Better performance, in terms of lower operating voltage and higher current density, can be achieved by further decreasing the size of the surface tunnel barrier of field emitter-based cold cathodes. The large piezoelectric field produced in pseudomorphically grown InGaN layers on GaN field emitter pyramids allows the reduction of the surface energy barrier. Experiments have shown that the amount of barrier lowering increases with increasing InGaN thickness up to some critical thickness where the effects of strain relaxation and scattering reduce the effect of the piezoelectric barrier lowering. Results of an experiment have shown an effective electron affinity of 1 eV, which is reduced 70% from the electron affinity of GaN, 3.5 eV. The effective of the electron affinity reduction is to reduce the turn-on voltage of the field emitter arrays, from 300 V to 150 V.

14. SUBJECT TERMS
GaN, field emitter array, vacuum microelectronics, integrated anode, piezoelectric effect pseudomorphic growth, InGaN, cold cathode

15. NUMBER OF PAGES
24

16. PRICE CODE

17. SECURITY CLASSIFICATION OF REPORT	18. SECURITY CLASSIFICATION OF THIS PAGE	19. SECURITY CLASSIFICATION OF ABSTRACT	20. LIMITATION OF ABSTRACT
UNCLASSIFIED	UNCLASSIFIED	UNCLASSIFIED	UL

• Table of Contents

• List of Illustrations and Tables

(1) List of Manuscripts

- R.D. Underwood, P. Kozodoy, H. Xing, S. Keller, J. P. Ibbetson, S.P. DenBaars, and U.K. Mishra, "InGaN/GaN Field Emitters with Lowered Effective Electron Affinity," to be presented at 12th International Vacuum Microelectronics Conference, Darmstadt, Germany, July 5-9, 1999.
- R.D. Underwood, P. Kozodoy, S. Keller, S.P. DenBaars, and U.K. Mishra, "Piezoelectric surface barrier lowering applied to InGaN/GaN field emitter arrays," *Appl. Phys. Lett.*, vol. 73 (3), pp. 405-407, 1998.
- R.D. Underwood, P. Kozodoy, S. Keller, S.P. DenBaars, and U.K. Mishra, "InGaN/GaN Field Emitters with a Piezoelectrically-Lowered Surface Barrier," presented at the 11th International Vacuum Microelectronics Conference, Asheville, NC, July 19-24, 1998, pp. 283-284.
- D. Kapolnek, S. Keller, R.D. Underwood, S.P. DenBaars, and U.K. Mishra, "Spatial control of InGaN luminescence by MOCVD selective epitaxy," *J. Crystal Growth*, vol. 189/190, pp. 83-86, 1998.
- R.D. Underwood, S. Keller, U. K. Mishra, D. Kapolnek, B. P. Keller, S. P. DenBaars, "GaN field emitter array with integrated anode," J. Vac. Sci. Technol. B, vol. 16 (2), pp. 822-825, 1998.
- R. D. Underwood, D. Kapolnek, B. P. Keller, S. Keller, S. P. DenBaars, and U. K. Mishra, "Selective-area Regrowth of GaN Field Emission Tips," *Solid-St. Electron.*, vol. 41, pp. 243-245, 1997. (Topical Workshop on III-V Nitrides, Nagoya, Japan, 21-23 Sept 1995, published in 1997, pp. 243-245)
- D. Kapolnek, S. Keller, R. Vetury, R. D. Underwood, P. Kozodoy, S. P. DenBaars, and U. K. Mishra, "Anisotropic epitaxial lateral growth in GaN selective area epitaxy," *Appl. Phys. Lett.*, vol. 71 (2), pp. 1204-1206, 1997.
- R. D. Underwood, D. Kapolnek, B. P. Keller, S. Keller, S. DenBaars, and U. Mishra, "Field Emission From Selectively Regrown GaN Pyramids," presented at 54th Device Research Conference, Santa Barbara, California, 1996, pp. 152-153.
- D. Kapolnek, R. D. Underwood, B. P. Keller, S. Keller, S. P. DenBaars, and U. K. Mishra, "Selective area epitaxy of GaN for electron field emission devices," *J. Crystal Growth*, vol. 170, pp. 340-343, 1997. (8th Int. Conf. on MOVPE, Cardiff, UK, 9-13 June 1996, pp. 340-343)

(2) Scientific Personnel & Degrees Earned

- Professors Umesh K. Mishra and Steven P. DenBaars.
- Post-doctoral researcher Stacia Keller.
- Graduate Students Robert Underwood, David Kapolnek, and Peter Kozodoy.

- David Kapolnek has submitted his Ph.D. dissertation entitled, "Selective epitaxy of gallium nitride and related materials by metalorganic chemical vapor deposition."
- Robert Underwood will complete his Ph.D. dissertation entitled, "Indium gallium nitride/gallium nitride vacuum microelectronic cold cathodes: Piezoelectric surface barrier lowering" in August 1999.

(3) Inventions

- Patent disclosures on InGaN/GaN field emitter arrays and AlGaN/InGaN/GaN planar cold cathodes submitted to UC patent office.

(4) Scientific Progress and Accomplishments

Statement of the Problem

Cold cathodes are essential for the realization of high current density, high efficiency microwave power devices. Cold cathodes do not require the heating of a filament and their current density can be higher than thermionic cathodes. Cold cathodes also have exciting potential uses in high-throughput parallel electron beam lithography and flat-panel displays. Many cold cathodes require the use of cesium to lower the surface energy barrier. Cesium is effective in this purpose but suffers from poor stability and short lifetime. Cold cathodes with small barriers without the use of cesium would have high current density, high efficiency *and* stability and robustness. The III-V nitrides are semiconductors that possess properties that make them suitable for cold cathode applications. These properties include high electron concentration, high thermal conductivity, low surface reactivity, and high hardness. These advantageous properties are the basis for our work on GaN-based cold cathodes. The cold cathode type investigated under this contract was GaN-based field emitter arrays. Field emitters use intense electric fields to liberate electrons from the cathode material into vacuum.

Summary of Important Results

Over the course of the project, several important results have been realized. These are listed below.

1) Growth, characterization, and optimization of selective, self-limited GaN field emitter arrays. Arrays of GaN pyramids (base diameter 2 μm) are grown by metalorganic chemical vapor deposition (MOCVD) on a masked template. Lithographically produced oxide masks determine the array pattern. The growth conditions have been determined such that the arrays are self-limited, i.e. the growth of the pyramids stops after the completion of the pyramid sidewalls. This self-limitation helps to mitigate the effects of growth non-uniformities present in the MOCVD system. Uniform arrays of pyramids are essential for uniform current density from a field emitter array.

2) The use of an integrated anode structure. The operating voltage of a field emitter array is determined by the sharpness of the emitter and the separation of the anode and the pyramids. Since the sharpness of the pyramids is fixed by the crystal geometry, lowering of the operating voltage is most easily accomplished by shrinking the device dimensions. This

was accomplished by using a microelectronic integrated anode over the field emitter array. The achievable separations between the anode and cathode were in the range of 0.5 to 1 μm.

3) Piezoelectric lowering of the surface energy barrier. In addition to the effects of geometry on the operating voltage of the field emitters, the surface energy barrier has a significant effect on the operating voltage. The surface energy barrier for a semiconductor field emitter is the electron affinity. By using a pseudomorphically grown layer of InGaN on the GaN field emitter pyramids, the effective electron affinity of the composite emitter was lowered by about 70% compared to the un-coated GaN field emitter arrays. The smallest effective electron affinities produced thus far have been approximately 1.0 eV for a coating of 500 Å of $In_{0.5}GaN$ on GaN pyramids.

The details of the GaN pyramid growth and integrated anode have been previously given in interim progress reports. The following section details the results related to the piezoelectric surface barrier lowering achieved over the final reporting period.

Paths to lowering the operating the voltage of field emitters include increasing the field enhancement, lowering the surface energy barrier height, and increasing the emission area. The two most important parameters are the surface barrier and the field enhancement factor because the emission current is exponentially related to both. The field enhancement factor can be increased by sharpening the emitters or making the device dimensions smaller as we showed previously with the integrated anode FEAs. The fact that the GaN field emitters grow constrained by the crystal geometry gives the benefit of uniformity but with the disadvantage that the pyramids have a large tip angle (~60°) and thus a relatively low field enhancement factor. Methods have been demonstrated in other material systems to sharpen the emitters, either by the effects of oxidation[1-3] or by ion-beam milling[4-6], but no such method has been demonstrated for the nitrides, and it is also not clear if the methods would produce arrays of sufficient uniformity for practical FEA devices.

Lowering the effective surface barrier of the emitters is another method to increase the current at a given voltage for field emitters. The most common method to lower the work function or electron affinity of materials is the application of an electropositive adsorbate to the surface of the material. The most common adsorbate for reducing the surface barrier is cesium, and the mechanism of the cesium work function lowering and an estimate of the magnitude of the effect are given briefly. The use of cesium has several drawbacks such as the requirement of UHV, migration of the cesium on the device, and possible compromising of the insulating components of the device. Herein, we present an overview of the piezoelectric effect in III-V nitride semiconductors, which forms the basis of a new method to produce a large dipole at the surface of a field emitter. The effect of this dipole in lowering the electron affinity of InGaN/GaN FEAs is the primary result of this project. Using a strained layer of InGaN on the GaN pyramids, a large dipole can be grown into the crystal structure that lowers the effective electron affinity. Because the dipole is built into the crystal structure of the emitter, it will not suffer from the stability problems that mobile adsorbates, such as Cs, suffer. Finally, experimental measurements of the current-voltage characteristics of InGaN/GaN field emitters that show strong support for the model are presented.

Surface Barrier Lowering Using Cesium

The use of electropositive adsorbates to lower the work function or electron affinity of materials has been investigated for cathode and photocathode applications.[7] The most technologically important electropositive adsorbates are the alkali metals, which are known to have low ionization potentials, and the most important of the alkali metals for surface barrier modification has been cesium. Cesium has the lowest ionization potential of any element. The physics behind the surface barrier lowering of cesium adsorbates is still not completely understood for all material systems. The simplest model treats the cesium atom-surface interaction by way of a charge transfer from the cesium to the substrate. This is schematically represented, using a tight-binding approach, in Figure 4.1(taken after Fig. 4.1 in [7]). When the Cs atom adsorbs on the substrate, the highest energy electron in the Cs atom can transfer to the substrate, leaving the Cs ionized. A dipole is formed at the surface and this dipole counteracts the work function barrier of the substrate. In fact, each Cs atom does not transfer a full electron to the substrate, but rather, the ionicity of the bond gives the fraction of the electronic charge transferred. The ionicity of the bond can be calculated from Pauling's electronegativity values for the elements. To calculate the order of magnitude of the charges involved in cesium-induced work function lowering, the case of GaAs will be considered

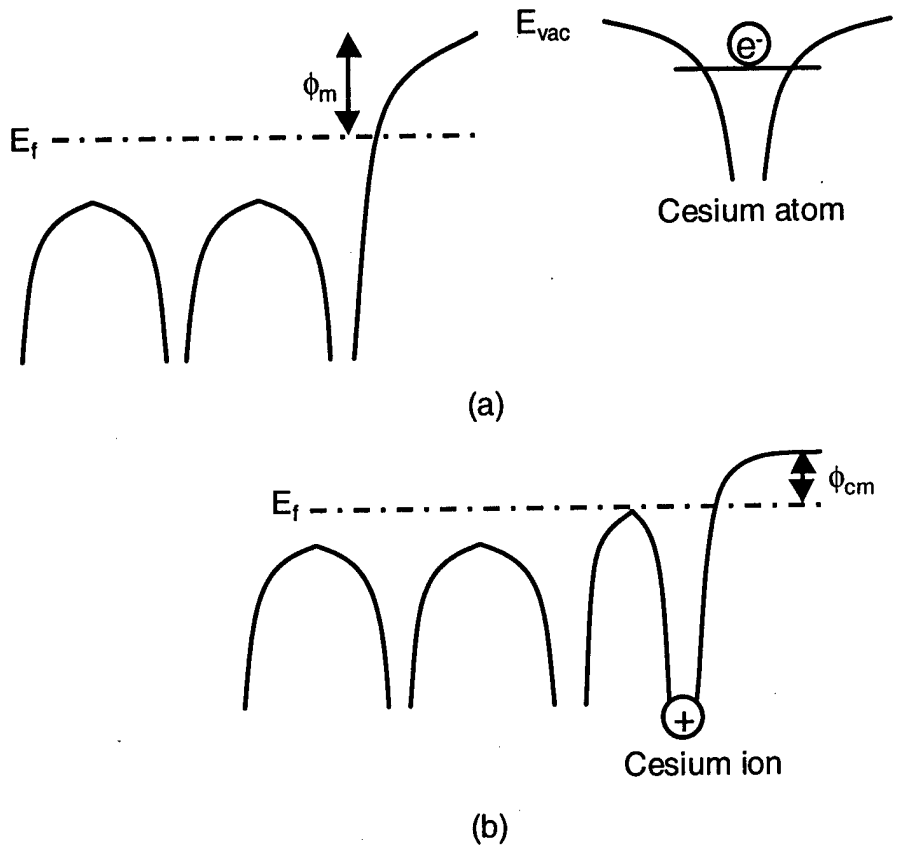

Figure 4.1. (a) Energy diagram of a separate metal surface and Cs atom with common vacuum level. The line on the Cs atom indicates the top-filled electron level. (b) As the Cs atom adsorbs on the metal surface, the Cs atom ionizes and the electron is transferred to the conduction band of the metal. The result is a surface dipole that counteracts the metal work function.

because it is a well-studied system. For Cs on Ga or Cs on As, the ionicity of the bonds is about 0.19 and 0.35 respectively. For Cs on a GaAs surface, the effective work function is 1.4 eV, which is about 2.6 eV less than a clean GaAs surface (4.0 eV).[8] The potential drop caused by a dipole is given by $\Phi_d = \rho_s l/\varepsilon_o$ where ρ_s is the sheet charge of the dipole, and l is the length of the dipole. As an approximation, the dipole length is taken to be the length of Cs-Cs bond, about 4 Å. The dipole charge necessary to produce this change in potential is about $3.6\times10^{13}q$ C/cm^2. Given that each Cs contributes only a fraction of a charge to the dipole, the density of Cs atoms necessary to produce this charge density is in the range of 1×10^{14} atoms/cm^2. This density is of the same order of the surface density of atoms of GaAs (4×10^{14} atoms/cm^2). Thus, we see that in order to produce a large change in the surface energy barrier, a charge density of the order of 10^{14} cm^{-2} is necessary. Although, the use of cesium is a good method to achieve such large work function reduction, the instability of Cs in the vacuum environment makes it an unsuitable technology for practical devices. A novel method to achieve dipoles of these magnitudes using the piezoelectric effect in the III-V nitrides will be the subject of the next two sections.

Piezoelectric Effect in Nitride Semiconductors

The piezoelectric effect was precisely defined by W.G. Cady as "electric polarization produced by mechanical strain in crystals belonging to certain crystal classes, the polarization being proportional to the strain and changing sign with it."[9] Stated mathematically, the relation between the electric polarization and the strain in the crystal (assuming no applied electric fields) is given by

$$P_i = e_{ij} S_j \qquad (4.1)$$

where P_i is the polarization in the i-direction (in units of C/m^2), e_{ij} are the piezoelectric stress constants (C/m^2), S_j are the strain tensor components (m/m), i=1,2,3 represents the three Cartesian directions, j ranges from 1 to 6, and the Einstein summation convention has been employed. The above equation can be identified as a tensor equation where the strain tensor is a 6-component tensor and the stress constants form a 3×6 tensor. The piezoelectric stress constant e_{ij} gives the polarization in the i-direction caused by a j-stress. For j=1,2,3 the stress is a simple compressive or extensive stress component corresponding to the same i-directions, but for j=4,5,6 the stress components are shearing stresses. The piezoelectric polarization can also be given in terms of the stress tensor, **T**, and the piezoelectric strain constants, d_{ij}, as

$$P_i = d_{ij} T_j \qquad (4.2)$$

where stress has units of N/m^2, and the units of the piezoelectric strain constants are given in C/N (or equivalently, m/V). Knowing that the strain and stress in a crystal are related through the elastic constants, c_{ij}, a relation between the piezoelectric strain and stress constants can be derived to yield

$$e_{mh} = \sum_{i=1}^{6} c_{ih} d_{mi} \qquad (4.3)$$

where the elastic constants carry the units of N/m^2. The above equations are the basic equations of piezoelectricity and the derivations are available in Cady's work cited above and other texts on piezoelectricity.[10, 11]

The piezoelectric polarization physically derives from the separation of charges that occurs when a strain or stress is applied to a crystal. In order for a uniform stress to induce the movement of the charges to produce an electric field, the crystal must not have a center of symmetry. Lack of a center of symmetry is the fundamental crystal characteristic that determines whether a crystal will be piezoelectric or not. As an example, a crystal from a

system with no symmetry at all, the triclinic system will have the maximum of 18 independent piezoelectric constants. Additional crystal symmetries reduce the number of non-zero piezoelectric constants. The III-V nitrides can be grown in either a cubic (zinc-blende) or a hexagonal (wurtzite) crystal system. The most common type of nitride is the hexagonal type. The symmetry of the hexagonal nitrides system is denoted by *6mm*, which indicates that it has a 6-fold rotation axis and two sets of mirror planes that contain the 6-fold axis.[12] The symmetry reduces the number of independent piezoelectric constants to three and the number of independent elastic constants to five. The elastic stiffness tensor and piezoelectric strain tensor for the hexagonal nitrides are given in Figure 4.2. The piezoelectric stress tensor has the same form as the piezoelectric strain tensor.

Strain in epitaxially grown semiconductors can be caused by either thermal expansion mismatch or lattice mismatch of the epitaxial layer and the substrate. In the initial growth of an epitaxial layer on a substrate of differing lattice constant, the epitaxial layer will grow with an in-plane lattice constant equal to that of the substrate. If the epitaxial layer's in-plane lattice constant is smaller than the substrate's, then the epitaxial layer will experience biaxial extensional strain in the growth plane. Conversely, if the epitaxial layer has a larger in-plane lattice constant than the substrate, the epitaxial layer will experience a biaxial compressional strain. To first order, the volume of the unit cell of the epitaxial layer will be the same as if the layer were grown with its natural lattice constant. Thus, extension in the growth plane will lead to compression in the growth direction, and compression in the growth plane will lead to extension in the growth direction. The above condition is termed pseudomorphic growth and is illustrated schematically in Figure 4.3. As the epitaxial growth is continued, the substrate's influence on the growth will weaken and dislocations will form to allow the epitaxial layer to grow with its bulk lattice constants. The formation of dislocations to reduce strain is termed relaxation, and relaxation limits the maximum thickness of pseudomorphic epitaxial layers.

The binary compounds, GaN, AlN, and InN form a compound semiconductor alloy system. AlN has the smallest *a*-plane lattice constant, followed by GaN, and finally InN with the largest. When thin, pseudomorphic layers of In_xGaN or Al_xGaN are grown on a thick layer of GaN oriented in the *c*-direction, the strain in the *a*-plane produces a piezoelectric field in the growth direction (the *c*-direction). The field can be derived by using the tensors given in Figure 4.2, equations (4.1), (4.2), and (4.3), and the relation between the polarization and

$$\mathbf{c} = \begin{bmatrix} c_{11} & c_{12} & c_{13} & 0 & 0 & 0 \\ c_{12} & c_{11} & c_{13} & 0 & 0 & 0 \\ c_{13} & c_{13} & c_{11} & 0 & 0 & 0 \\ 0 & 0 & 0 & c_{44} & 0 & 0 \\ 0 & 0 & 0 & 0 & c_{44} & 0 \\ 0 & 0 & 0 & 0 & 0 & \frac{1}{2}(c_{11}-c_{12}) \end{bmatrix}$$ Elastic Stiffness Tensor

$$\mathbf{d} = \begin{bmatrix} 0 & 0 & 0 & 0 & d_{15} & 0 \\ 0 & 0 & 0 & d_{15} & 0 & 0 \\ d_{31} & d_{31} & d_{33} & 0 & 0 & 0 \end{bmatrix}$$ Piezoelectric Strain Tensor

Figure 4.2. Tensors for evaluation of piezoelectric effects for crystals with 6mm symmetry.

field, $F_3 = -P_3 / \varepsilon_r \varepsilon_o$. The relation for the field is given in the literature[13-16] and is repeated here,

$$F_3 = -\frac{2d_{31}}{\varepsilon_r \varepsilon_o}\left(c_{11} + c_{12} - 2c_{13}^2 / c_{33}\right) S_1 \qquad (4.4)$$

where S_1 is the biaxial strain (i.e. S_1=S_2).

The sign of the terms in equation (4.4) are crucial to determining the direction of the field. First, the strain is defined as positive for an extensional strain and negative for compression. The sign of the piezoelectric constant is positive if the positive piezoelectric charge is induced in the positive direction by a positive strain.[11] For MOCVD-grown nitrides, the surfaces appear to be metal-terminated[17] and the growth direction is [0001] where the positive growth direction is defined, by convention, as pointing from the group-III element to the group-V element between basal planes.[17]

The magnitude of the piezoelectric field is also dependent on the growth direction of the InGaN layer on the GaN layer. The above equation (4.4) is valid for growth of the template and InGaN layer in the *c*-direction. Bykhovski *et al.* have made an analytical calculation for off-polar-axis growth.[13] Their calculation matches the lattice constants in the growth plane for any angle of growth. The results indicate that the largest piezoelectric effects are realized for growth in the *c*-direction, and the sign of the piezoelectric field changes sign at a certain angle, and finally, the polar piezoelectric field goes to zero for growth perpendicular to the polar axis. Figure 4.4 shows the relative piezoelectric polarization in the *c*-direction as a function of the angle between the *c*-axis and the growth direction. The calculations were made using a finite-element mechanical structure simulator, ABAQUS.[1] The crystal properties were entered into the simulation file and bar of GaN was subjected to a biaxial extensional stress of 10 GPa. In addition to calculating the strain and displacement of the crystal, if the piezoelectric properties of the crystal are included, the resulting potential and piezoelectric charge distribution can be simulated. The figure shows the same shape as the result of Bykhovski *et al.* Because of the large radius of the field emitter tips in this work, the emission is assumed to originate from planes nearly parallel or at only a slight angle to the (0001) plane, so that equation (4.4) can be used for the magnitude of the piezoelectric charge in this dissertation.

The strain-induced piezoelectric fields alter the electrical and optical properties of the nitrides with respect to their bulk properties. The piezoelectric properties and their effects on electrical and optical devices have been an active area of research for the past half-decade. Bykhovski *et al.* have studied the effects of piezoelectric fields on the charge distribution and conduction characteristics of GaN-AlN-GaN structures and the piezoresistive effects in

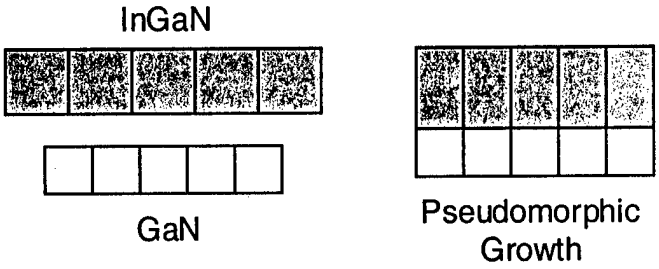

Figure 4.3. Illustration of the lattice dimension changes representative of pseudomorphic growth.

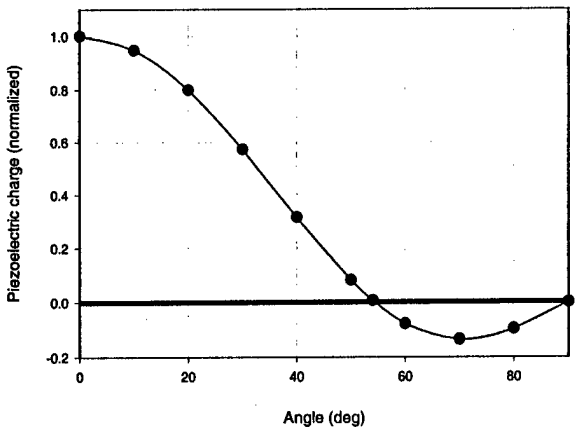

Figure 4.4. Normalized piezoelectric charge versus polar angle simulated using ABAQUS™ finite element program.

GaN.[13, 14, 18-20] Martin *et al.* have shown that piezoelectric effects must be considered when trying to determine the band offsets of nitride heterostructures.[15] Band-bending caused by piezoelectric fields has been suggested to explain the high amount free channel charge in un-doped nitride field-effect transistors.[21-30] Yu *et al.* have studied the piezoelectric effects on Schottky barrier heights.[31, 32] The effect of the piezoelectric fields on the optical properties of the nitride semiconductors are also an active topic of research.[16, 33-43] The next section will present a calculation of the effect of the piezoelectric field produced in a pseudomorphic layer of InGaN on the field emission from GaN FEAs.

Surface Barrier Lowering in InGaN/GaN Field Emitters

A piezoelectric field in an epitaxial semiconductor produces a linear change in the potential of the conduction and valence bands. For a strained layer of InGaN grown on a thick GaN layer, the resulting band diagram is depicted in Figure 4.5. The *a*-plane lattice constant of InGaN is larger than that of GaN, thus the InGaN experiences a compressional strain. The positive direction in the figure is the growth direction, [0001]. The piezoelectric constants of the hexagonal nitrides have a negative sign, thus a positive strain produces a negative charge in the positive direction (see references given in Appendix B). Because the strain in this case is negative, the resulting charge at the InGaN/vacuum interface is positive. An equal amount of negative charge is induced at the GaN/InGaN interface. Thus, the piezoelectric field points in the negative direction, $[000\bar{1}]$ in this case. The piezoelectric field produces a decreasing slope in the band diagram. Consequently, the vacuum level at the surface of the InGaN is reduced relative to the vacuum level of the GaN. If band bending in the GaN and the filling of the InGaN conduction band by electrons from the GaN is ignored, the amount of potential drop is equal to the piezoelectric field multiplied by the thickness of the InGaN layer.

In reality, the band bending and filling of the InGaN conduction band must be considered to accurately calculate the band diagram of the GaN/InGaN layers. We chose to calculate the bands numerically using a band calculation program, BandProf.[2] The BandProf

[1] ABAQUS™ is a registered trademark of Hibbitt, Karlsson & Sorensen, Inc., 1080 Main Street, Pawtucket, RI 02860-4847.

[2] W. R. Frensley, BandProf, © University of Texas at Dallas.

program allows the input of material parameters such as band offsets, effective masses, and dopant energy levels. The values used for the material parameters of InN and GaN are given in Appendix B and the valence band offset between InN and GaN was taken as $\Delta E_v = 0.46\Delta E_g$, which is an average of the offsets given in Ambacher.[44] Estimation of the material parameters for InGaN are made using Vegard's law (linear interpolation of the values of GaN and InN). In the BandProf program, the only way to introduce fixed charge is by the use of dopants. The piezoelectric charge is introduced into the description of the material by the use of two fictitious "dopants." Dopant *A*, is given an energy level 1.5 eV above the conduction band minimum (a donor), and thus, is always ionized with a positive charge. Dopant *B*, is given an energy level 1.5 eV below the valence band maximum (an acceptor), and thus, is ionized with a negative charge. Finally, a fictitious material was created to simulate vacuum. The conduction band of the fictitious material simulated the vacuum level and thus the conduction-band offset of the "vacuum" material with respect to GaN was set equal to the electron affinity of GaN.

The epitaxial layer structure to be studied is input to BandProf by specifying the layers in a text file. Each layer is specified by the composition of the semiconductor, the thickness of the layer, and the doping type and amount, if any. At the InGaN/GaN interface, a small layer (two times the mesh size of 0.5 Å) is doped with dopant *B* to a volume charge density equivalent to the piezoelectric surface charge density. At the InGaN/vacuum interface, an equivalent charge is introduced by doping the surface with dopant *A*. To calculate the necessary piezoelectric charge, first the strain must be calculated. The strain is given by the lattice mismatch of the *a*-plane lattice constant,

$$S_1 = \frac{a_{epi} - a_{sub}}{a_{epi}}, \qquad (4.5)$$

where a_{epi} is the lattice constant of the strained layer and a_{sub} is the lattice constant of relaxed substrate layer. Using Vegard's law to calculate the *a*-lattice constant for In_xGaN, the strain for an In_xGaN layer grown on a relaxed GaN layer can be calculated from

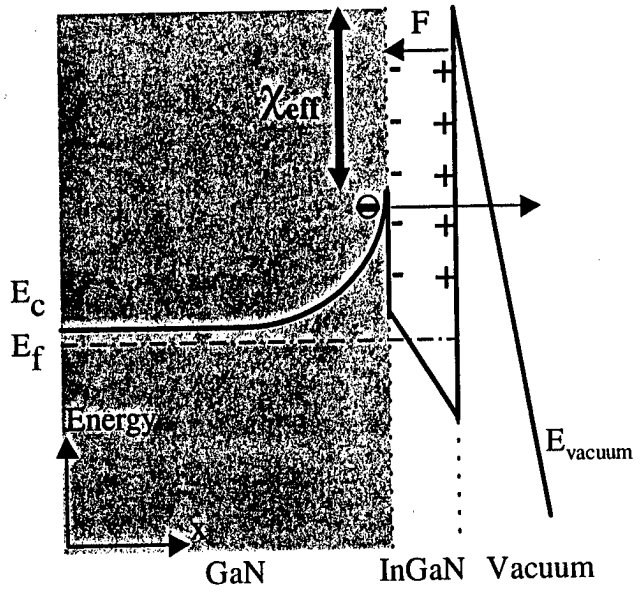

Figure 4.5. Schematic conduction band diagram of InGaN/GaN field emitter. Electrons travel ballistically across the InGaN layer and, thus, effectively tunnel from the maximum of the GaN conduction band edge at the GaN/InGaN interface. The vacuum level is shown for an applied bias.

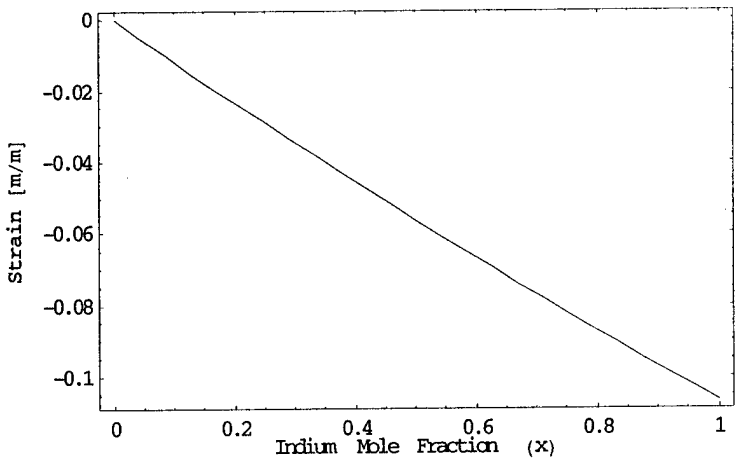

Figure 4.6. Strain in pseudomorphic In_xGaN layer as a function of In mole fraction, x.

$$S_1 = \frac{(a_{GaN} - a_{InN})x}{a_{GaN} + (a_{InN} - a_{GaN})x}, \qquad (4.6)$$

where x is the In mole fraction. A plot of equation (4.6) over range from x=0 to 1.0 is given in Figure 4.6. The strain varies from 0 to about -10% over that range of In mole fraction. Now that the strain has been calculated, the field and charge can be calculated using equation (4.4), using Vegard's law to calculate the elastic and piezoelectric constants for the In_xGaN. The piezoelectric polarization charge ranges from 5.8×10^{12} cm^{-2} for 5% In concentration to 5.1×10^{13} cm^{-2} for 90% In concentration. Note that these charge concentrations are in the same range as calculated for the Cs work function lowering (3.6×10^{13} cm^{-2}) presented in section (4.2).

The band diagrams calculated by the BandProf simulations are similar to the schematic shown in Figure 4.4. A series of calculated band diagrams, for 5% In concentration and InGaN layer thickness from 5-100 nm, are shown in Figure 4.7. The field emission current from the GaN/InGaN structure could be calculated, in theory, by numerically integrating the transmission and supply functions based on the potentials given by BandProf, however, a physical argument leads to a simple interpretation of the effects of the InGaN layer. The main effect of the InGaN layer is to lower the vacuum level at the surface and raise the conduction band minimum at the InGaN/GaN interface. The energy difference between the surface vacuum level and the conduction band minimum at the GaN/InGaN interface can be seen to be equivalent to an effective electron affinity, χ_{eff}. This effective electron affinity will be less than the electron affinity of GaN if the InGaN is strained and the piezoelectric field exists. In this approximation, the Fowler-Nordheim current-voltage relation can be simply modified by replacing the electron affinity, χ, by the effective electron affinity, χ_{eff}

$$I = AV^2 \exp\left(-\frac{B\chi_{eff}^{3/2}}{\beta V}\right). \qquad (4.7)$$

BandProf simulations of the effect were calculated for In compositions ranging from 5% to 90% and InGaN layer thickness from 0 to 100 nm. The results of the calculations are given in Figure 4.8. The plot shows the effective electron affinity as a function of InGaN thickness with the In mole fraction as a parameter. The effect of increasing the InGaN thickness is to increase the length over which the piezoelectric field acts, which increases the total electron affinity change. Increasing the In concentration increases the strain, which increases the piezoelectric field strength. The increased dipole strength increases the surface

barrier lowering. The saturation of the effective electron affinity at increased InGaN thickness and In mole fraction is the result of the mobile charges transferred from the GaN accumulating at the InGaN/vacuum interface. The minimum value of the electron affinity is seen to be slightly less than 0, which indicates that it may be possible to produce a negative electron affinity with this method. The saturation of the effective electron affinity occurs at lower layer thickness with increasing In composition. For In concentrations above 10%, the lowering effect is strongest for InGaN thickness between 20 Å and 200 Å, and additional InGaN thickness does not greatly reduce the effective electron affinity.

Three effects limit the maximum reduction that can be achieved. These effects are strain relaxation, electron mean free path, and the depletion of the GaN layer. The first is the requirement that the InGaN film remains strained in order for the piezoelectric effect to exist. As the thickness of a strained layer increases, the film will relax through dislocations to relieve the strain. A critical thickness can be defined as the thickness where the film has relaxed so that it has its own bulk lattice constant. Simple calculations, such as those based on

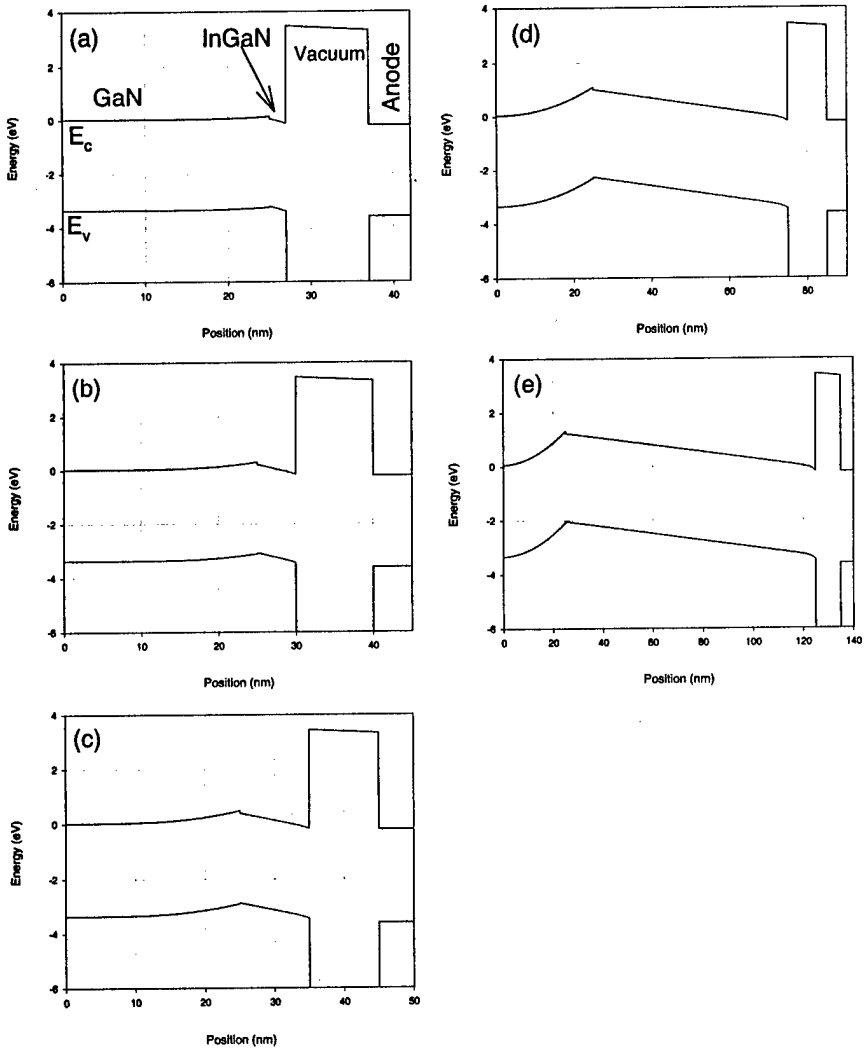

Figure 4.7. Calculated band diagram of InGaN/GaN field emitters. The growth direction is to the right. The InGaN layer can identified by the downward sloping region directly in front of the vacuum region. The In concentration is 5% and the InGaN thickness is varied from 5 to 100 nm (a)-(e). In this figure, the Fermi level is at 0 eV.

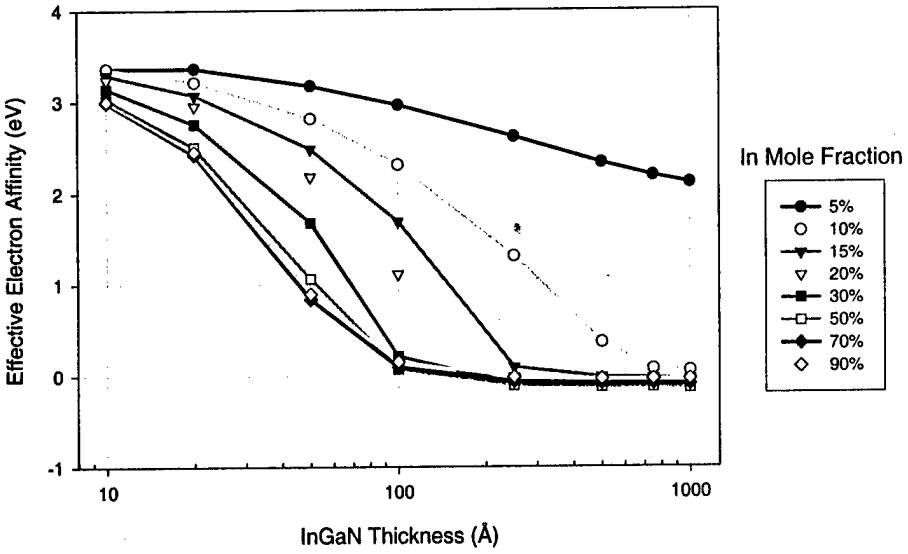

Figure 4.8. Calculated effective electron affinity of InGaN/GaN field emitters as a function of InGaN thickness with the In mole fraction as a parameter.

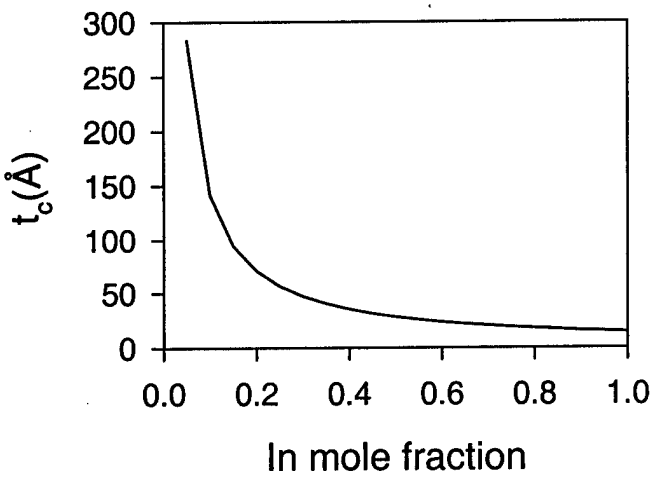

Figure 4.9. Simple estimation of the critical thickness of InGaN on GaN.

the Matthew-Blakeslee model, predict that only extremely thin strained InGaN layers can be grown (less than 100 Å).[16, 45] A simple estimation of the critical thickness can be given by the expression $t_c = a_{sub}^2/2(\Delta a)$, where t_c is the critical thickness, a_{sub} is the substrate a-plane lattice constant and Δa is the lattice mismatch. A plot of this function for InGaN on GaN is given in Figure 4.9, and shows that the critical thickness for In concentrations above 5% is limited to less than 30 nm. Experimental evidence suggests that strained InGaN layers can be grown to larger thickness than the simple models suggest.[16, 46]

The second effect that can limit the effectiveness of the InGaN layer is scattering of the electrons in the layer. The above assumption of an effective electron affinity essentially relies on ballistic transport of the electrons through the InGaN. If the thickness of the InGaN layer is larger than the mean free path of electrons in InGaN, the scattering of the electrons will lose energy until they reach the InGaN conduction band minimum. Because the electron affinity of InGaN is larger than the electron affinity of GaN, the scattered electrons will have

a much lower probability of tunneling through the InGaN/vacuum barrier than electrons traveling ballistically through the InGaN. As the thickness of the InGaN increases, a greater fraction of the electrons will scatter in the InGaN layer, thus limiting the electron emission. Theoretical and Monte Carlo calculations of scattering in the nitride semiconductors indicate that the dominant scattering mechanism is polar optical phonon scattering. The Monte Carlo simulations of the channel regions of GaN FETs have shown that the electrons will thermalize to the conduction band in 200 to 400 Å.[3] Ye *et al.* have measured a polar optical phonon emission time of 0.2 ps for GaN.[47] For an electron velocity of 10^7 cm/s, the resulting relaxation length is 200 Å, which shows reasonable agreement with the theory. The above data are taken from studies of hot electron relaxation in GaN and provided a best current estimate for the mean free path, as a literature search yielded no references to similar studies for InGaN.

The final effect that can limit the validity of our model is the barrier caused by the large depletion in the GaN layer as a result of the piezoelectric effect in the InGaN, for thick InGaN layers. This upward bending of the bands can be clearly seen in Figure 4.7. Under

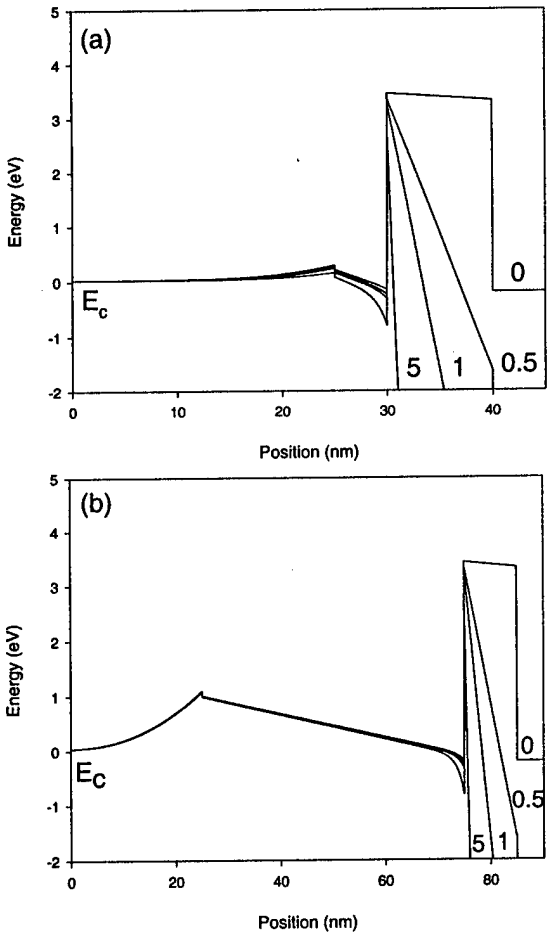

Figure 4.10. Effect of field penetration on the conduction band of the InGaN/GaN FEAs demonstrating the limitation of the effective electron affinity model. (a) 5% In, 50 Å InGaN. (b) 5% In, 500 Å. The numbers next to the profiles indicate the applied electric field in units of V/nm.

[3] J. Singh, private communication, 1999.

operation, the field penetration of the applied electric field can cause increased band bending near the surface. For thin layers (<100 Å) the field can penetrate sufficiently to decrease the barrier and allow electron transport. This is illustrated in Figure 4.10, where BandProf simulations with a bias applied to the anode (but no current flow) are shown. For 50 Å of $In_{0.5}GaN$ (Figure 4.10(a)), the field penetration causes the bands to bend sufficiently to allow the application of the effective electron affinity model. For a thicker InGaN layer (500 Å), the field can not penetrate sufficiently to cause appreciable band bending at the barrier and the effective electron affinity model should not be applicable. BandProf simulations are limited to zero current flow, and dynamic effects may have an effect not indicated here.

InGaN/GaN Field Emitter Results

InGaN/GaN field emitter arrays were grown and fabricated as discussed for the integrated-anode GaN field emitter arrays previously reported. The InGaN layers were grown on the GaN pyramids immediately after the GaN pyramid growth and were not intentionally doped. The thickness of the InGaN layer on the pyramids is difficult to measure. The thicknesses reported herein are estimated based on growth time and the enhanced growth rate of the pyramids versus planar films. The growth rate of InGaN on the sidewalls was grossly estimated to be four times the planar growth rate. Consequently, the absolute values of the thickness are not known, but the relative thickness of the InGaN layers can be assumed based on the growth times.

The first set of emitters grown to test the electron affinity lowering effect included a GaN FEA control, and two InGaN/GaN FEAs, one with InGaN thickness of 100 nm and the other with InGaN thickness of 200 nm. The In mole fraction was 15% as measured by x-ray diffraction on a planar InGaN region of the sample, provided by Giacinta Parish. The GaN field emitter exhibited a turn-on of about 175 V, emitters from the 100-nm InGaN sample showed a turn-on ranging from 63-123 V. The 200-nm emitter showed the highest turn-on of about 220-225 V. Each of the arrays had 5 tips and the anode-cathode separation was 2.8 μm for the 100-nm InGaN sample and 2.5 μm for the 200-nm InGaN sample and the control. Processing difficulties caused by large non-uniformity of the planar GaN template layers lead to geometrical differences in the FEA pyramids and, thus, the magnitude of the electron affinity reduction could not be accurately determined. Qualitatively, the reduction of the turn-

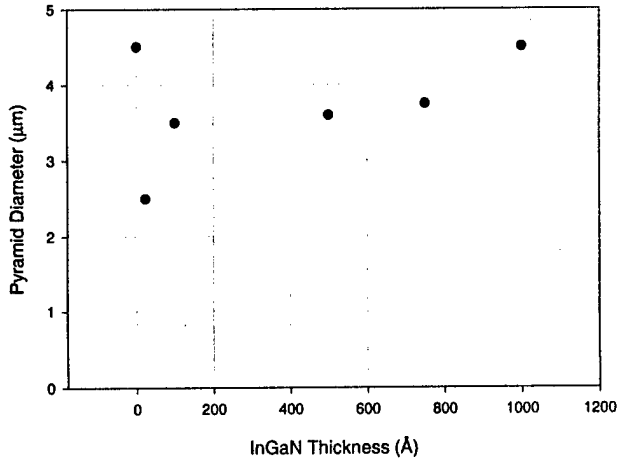

Figure 4.11. Variation of the pyramid base width for samples of differing InGaN layer thickness.

on voltage for the 100-nm sample was encouraging. At a thickness of 1000 Å, the theoretical effective electron affinity for 15% In is -0.4 eV. Although the turn-on of 63 V from this sample was the lowest turn-on voltage for a nitride-based FEA measured, the turn-on expected for such small effective electron affinity would be much lower. This thickness is somewhat above the calculated values of the mean free electron path discussed above, so that it may be suggested that scattering effects would increase the turn-on voltage. A second set of InGaN/GaN FEAs with more thickness points and less processing variation was fabricated to further investigate the effect.

In the second set of InGaN field emitters, InGaN layers of 20, 100, 500, 750, and 1000 Å were grown. The growth conditions of the MOCVD system had changed since the above-reported growth, and the In mole fraction was about 3-5% as measured by x-ray diffraction analysis, provided by Amber Abare, of a planar region on the 1000 Å sample. Thickness fringes in the x-ray measurements indicated a thickness of the planar film of 274 Å, which was very close to the target planar region thickness for the 1000 Å sample. This indicated that at least the control over the planar growth rate of the InGaN was very good. In contrast, the variation of the pyramid sizes was not as good as for past arrays. Over a single sample, the base width of the pyramids was observed to vary by as much as 20%. To

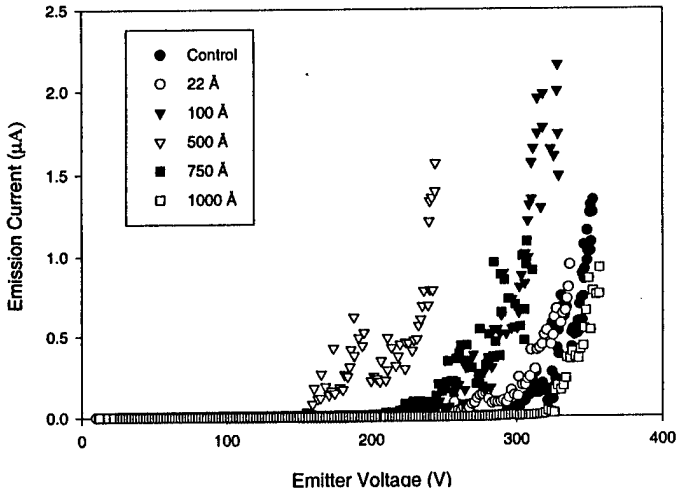

Figure 4.12. Current-voltage characteristics of $In_{0.05}GaN$/GaN FEAs.

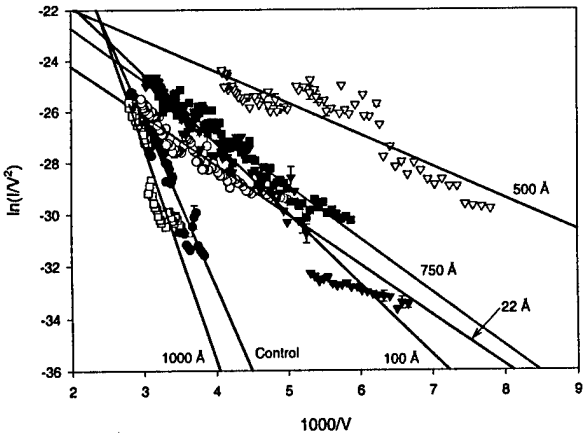

Figure 4.13. Fowler-Nordheim plots of emission data given in Figure 4.12.

determine the sample-to-sample variation, the base width of pyramids from the center of each sample was measured. The variation is shown in Figure 4.11, where the base width of the pyramids is plotted versus the target InGaN thickness (essentially, this is versus growth time). The variation of the base width among the samples is also about 20%. Other than the control sample, the base width increases with growth time although at a greater rate than would be expected from the target InGaN thicknesses. The pyramids from each sample were complete as observed in the SEM.

Current-voltage characteristics of the InGaN/GaN field emitters were performed using a high voltage source and picoammeter. From the emission current measurements, given in Figure 4.12, the turn-on voltage was measured and the Fowler-Nordheim plots (F-N plots) were constructed (see Figure 4.13). All of the emission characteristics reported in this section came from arrays that showed a linear F-N plot with a negative slope, and reverse leakage current at least three orders of magnitude below the forward current. From the slope of the F-N plots, the either the field enhancement or effective electron affinity could be calculated. The field enhancement factor of the control device was estimated by assuming that the electron affinity of the control was 3.5 eV. To check the reasonableness of this assumption, the geometry of the integrated anodes were observed by SEM observation.

The two most important geometrical parameters were the tip sharpness and the anode-cathode separation. Since the tips were all grown to completion, the radius of all of the tips was assumed to be 90 nm. The fitted field enhancement factor of the control sample was 67,000 cm^{-1} and using the concentric sphere model[51], the resulting k factor is 1.77, which is in the acceptable range for the model. The field enhancement factors calculated from the InGaN samples using their individual anode-cathode separations and the same k factor extracted from the control sample yields only a 7% variation among the FEAs (see Table 4.1). Because the emission current depends exponentially on the field enhancement factor, this variation may cause a large change in the current voltage characteristic; however, the variation in anode-cathode separation was random from device to device so that no trend could be clearly observed from the geometrical data.

The same field enhancement factor as the control is assumed to apply to the InGaN/GaN FEAs. The effective electron affinity of each of the InGaN/GaN FEAs was then calculated from the slope of the F-N plots using the common field enhancement factor. Table 4.2 contains the turn-on voltages, slope and intercept of the fits to the F-N plots, and the calculated effective electron affinities and emission areas. The goodness of the fit is given by the adjusted R^2 figure, also given in Table 4.2, with a value closer to one indicating a better

Table 4.1. Measured Anode-Cathode Separations and Theoretical Field Enhancement Factors (k=1.77).

InGaN Thickness (Å)	*Anode-Cathode Separation* (μm)	*Field Enhancement, β* (cm^{-1})
0	1.38	67,000
22	3.20	64,590
100	2.71	64,928
500	1.77	66,139
750	1.98	65,765
1000	0.73	71,665

Table 4.2. Measured and Calculated Data from InGaN/GaN FEAs.

InGaN Thickness (Å)	*Turn-on Voltage* (V)	*F-N Intercept*	*F-N Slope*	R^2_{adj}	β (cm^{-1})	*Emission Area* (cm^2)	χ_{eff} (eV)
0	290	-7.3±0.8	-6300±200	0.91	67000±2000	3×10^{-8} $\pm2\times10^{-8}$	3.5*
22	214	-20.2±0.4	-1970±90	0.86		4×10^{-15} $\pm2\times10^{-15}$	1.61±0.02
100	210	-16.8±0.3	-2590±60	0.95		2.5×10^{-13} $\pm0.7\times10^{-13}$	1.93±0.01
500	146	-20.3±0.5	-1030±90	0.69		5×10^{-16} $\pm3\times10^{-16}$	1.04±0.04
750	200	-18.5±0.3	-2070±70	0.94		2.5×10^{-14} $\pm0.8\times10^{-14}$	1.66±0.01
1000	313	-4.5±2.1	-7700±700	0.80		6×10^{-7} $\pm13\times10^{-7}$	3.9±0.2

*The electron affinity for the control is assumed 3.5 eV, and the field enhancement factor, β, is calculated from the equation for the F-N slope. This field enhancement is assumed for all of the InGaN samples to calculate the effective electron affinities.

fit. Figure 4.14 is a plot of the experimentally determined effective electron affinity versus InGaN thickness, shown along with the calculated theoretical effective electron affinities from Figure 4.8. Except for the point at 20 Å, the experimental points seem to follow the trend of the 5%-10% In calculations up to an InGaN thickness of 500 Å. From 500 Å to 1000 Å, the effective electron affinity increased, possibly from the aforementioned relaxation or scattering in the thicker layers. The minimum effective electron affinity achieved in this set of samples was the 1.04 eV from the sample with 500 Å of InGaN. The reduction of the effective electron affinity by 2.46 eV relative to the electron affinity of GaN represents a 70% reduction. The observation of lowering at InGaN thicknesses up to 500 Å does not agree with the above-mentioned limitations concerning the field penetration and the energy barrier in the GaN. This disagreement is not understood at this time, but may be attributable to incomplete knowledge of the InGaN thickness and unknown surface states.

The turn-on voltages of the InGaN/GaN field emitters were also measured from the current-voltage characteristics of the FEAs. Figure 4.15 shows the experimentally measured turn-on voltages and theoretical calculations of the turn-on voltage of field emitters with the theoretical effective electron affinities calculated for In percentage of 5 and 10%. The trend of the experimental turn-on voltages follows the 5% In theoretical calculation up to an InGaN thickness of 500 Å and then begins to increase. Interestingly, the turn-on voltage measured for the 1000 Å InGaN FEA is very close to the theoretically calculated turn-on voltages expected for emission from relaxed, bulk InGaN of 5 or 10% In composition.

In order to avoid array-damaging vacuum arcs, the InGaN/GaN FEAs were typically measured up to currents of 1-2 μA. If the current increase above this limit, a destructive arc often terminated the measurements of the arrays. A few of the arrays were tested using the curve tracer to determine the maximum current before failure. In all of the destructive tests, the device failed as a short. An array with 100 Å of InGaN showed maximum emission current of 9.8 μA from a 10-tip array at 372 V. The arrays with the smallest turn-on voltage, the 500 Å InGaN, showed the highest current capacity. Figure 4.16 shows a screen shot of the curve tracer showing a maximum current of about 19 μA at 310 V from a 10-tip array. The FEAs with 750 Å of InGaN display a maximum current of 1.9 μA at 334 V from a 10-tip array and 3.6 μA at 344.5 V from a 40-tip array. Finally, a 10-tip array with 1000 Å of InGaN showed a maximum current of 1.8 μA at 417.5 V. From the current-voltage pairs

given above, the power being delivered to the anode at the maximum current can be calculated. For the low turn-on, high current samples with thin InGaN, the anode power at breakdown was 3.65 mW (100 Å) and 5.89 mW (500 Å). For the thicker InGaN samples, the anode power at breakdown was lower, 0.64 mW (750 Å) and 0.75 mW (1000 Å). If the breakdown of these samples were being initiated by the destruction of the anode, it would be expected that the anode power would be about the same. This difference between the thin InGaN samples, where most of the electrons are assumed to travel ballistically through the undoped InGaN, and the thick InGaN samples, where the electrons will have a higher chance of scattering, suggests that the InGaN layer may have a role in determining the maximum current capability of the InGaN/GaN FEAs. More research will be necessary to test this hypothesis.

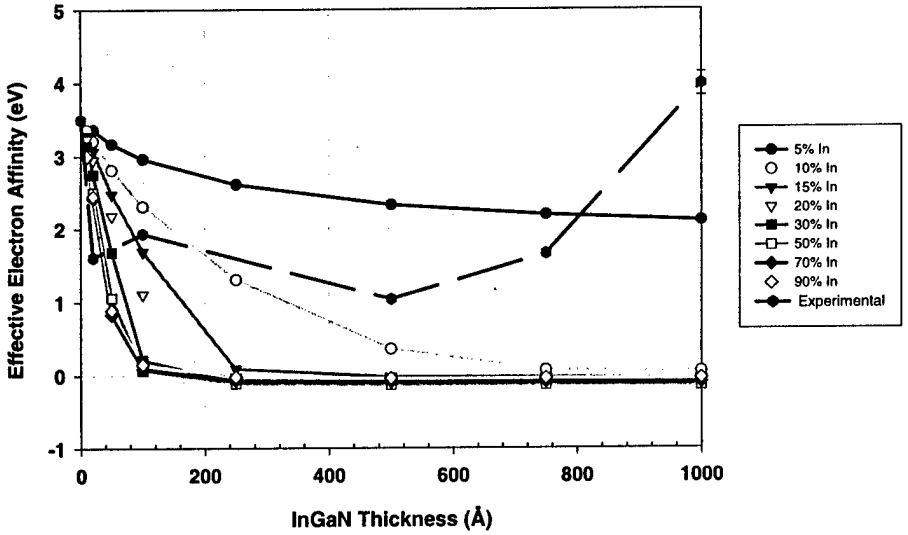

Figure 4.14. Experimental effective electron affinity of the InGaN/GaN FEAs (dashed line with hexagonal symbols) compared the theoretical effective electron affinities.

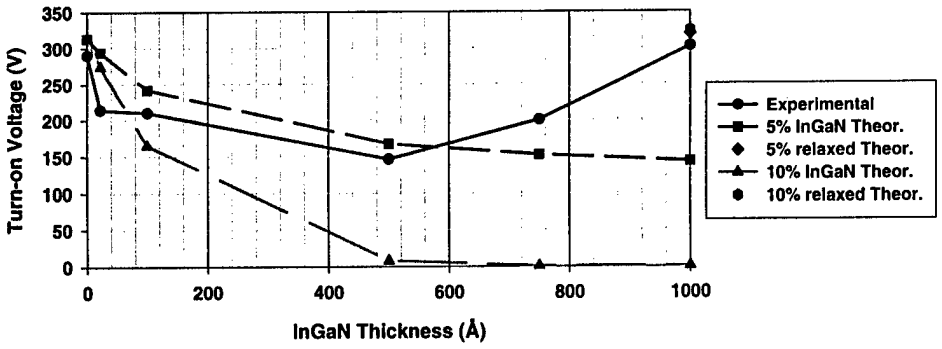

Figure 4.15. Experimental turn-on voltage (solid) and the theoretical turn-on voltages (dashed) calculated for 5 and 10% In composition InGaN/GaN FEAs. Also plotted on the right side, are two points calculated assuming the 5 and 10% InGaN layers are relaxed.

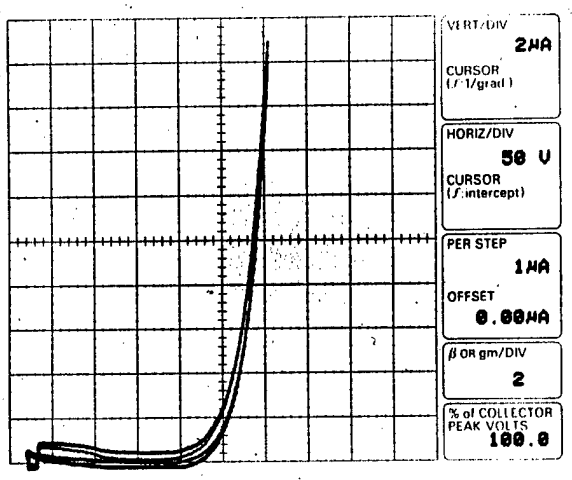

Figure 4.16. Picture of curve tracer screen with highest emission current observed for InGaN/GaN FEAs with 500 Å InGaN.

References

[1] R.B. Marcus and T.T. Sheng, "The Oxidation of Shaped Silicon Surfaces," *J. Electrochem. Soc.*, vol. 129, pp. 1278-1282, 1982.

[2] T.S. Ravi, R.B. Marcus, and D. Liu, "Oxidation sharpening of silicon tips," *J. Vac. Sci. Technol. B*, vol. 9, pp. 2733-2737, 1991.

[3] L.N. Yadon, D. Temple, C.A. Ball, W.D. Palmer, J.E. Mancusi, D. Vellenga, G.E. McGuire, C.M. Tang, H.F. Gray, and J.L. Shaw, "Pre- and Post-Metal Oxidation Sharpening Effects on Silicon Field Emitter Devices," in *Technical Digest of the 8th International Vacuum Microelectronics Conference*, 1995, pp. 197-201.

[4] O. Auciello, L. Yadon, D. Temple, J.E. Mancusi, G.E. McGuire, E. Hirsch, H.F. Gray, and C.M. Tang, "Ion Bombardment Sharpening of Field Emitter Arrays," in *Technical Digest of the 8th International Vacuum Microelectronics Conference*, 1995, pp. 192-196.

[5] A.P. Janssen and J.P. Jones, "The sharpening of field emitter tips by ion sputtering," *J. Phys. D: Appl. Phys.*, vol. 4, pp. 118-123, 1971.

[6] A.N. Stepanova, E.I. Givargizov, L.V. Bormatova, V.V. Zhirnov, E.S. Mashkova, and A.V. Molchanov, "Preparation of ultrasharp diamond tip emitters by ion-beam etching," *J. Vac. Sci. Technol. B*, vol. 16, pp. 678-680, 1998.

[7] R.L. Bell, *Negative electron affinity devices*. Oxford,: Clarendon Press, 1973.

[8] S.M. Sze, *Physics of semiconductor devices*, 2nd ed. New York: Wiley, 1981.

[9] W.G. Cady, *Piezoelectricity*, 1st ed. New York, NY: McGraw-Hill Book Co., 1946.

[10] W.P. Mason, *Piezoelectric Crystals and Their Application to Ultrasonics*. New York, NY: D. Van Nostrand Company, Inc., 1950.

[11] T.o. Ikeda, *Fundamentals of piezoelectricity*, Corrected pbk. ed. Oxford ; New York: Oxford University Press, 1996.

[12] N.W. Ashcroft and N.D. Mermin, *Solid state physics*. New York,: Holt Rinehart and Winston, 1976.

[13] A. Bykhovski, B. Gelmont, and M. Shur, "Strain and charge distribution in GaN-AlN-GaN semiconductor-insulator-semiconductor structure for arbitrary growth orientation," *Appl. Phys. Lett.*, vol. 63, pp. 2243-2245, 1993.

[14] A. Bykhovski, B. Gelmont, and M. Shur, "The influence of the strain-induced electric field on the charge distribution in GaN-AlN-GaN structure," *J. Appl. Phys.*, vol. 74, pp. 6734-6739, 1993.

[15] G. Martin, A. Botchkarev, A. Rockett, and H. Morkoç, "Valence-band discontinuities of wurtzite GaN, AlN, and InN heterojunctions measured by x-ray photoemission spectroscopy," *Appl. Phys. Lett.*, vol. 68, pp. 2541-2543, 1996.

[16] T. Takeuchi, S. Sota, M. Katsuragawa, M. Komori, H. Takeuchi, H. Amano, and I. Akasaki, "Quantum-confined Stark effect due to piezoelectric fields in GaInN strained quantum wells," *Jpn. J. Appl. Phys.*, vol. 36, pp. L382-385, 1997.

[17] F.A. Ponce, D.P. Bour, W.T. Young, M. Saunders, and J.W. Steeds, "Determination of lattice polarity for growth of GaN bulk single crystals and epitaxial layers," *Appl. Phys. Lett.*, vol. 69, pp. 337-339, 1996.

[18] A. Bykhovski, B. Gelmont, M. Shur, and A. Khan, "Current-voltage characteristics of strained piezoelectric structures," *J. Appl. Phys.*, vol. 77, pp. 1616-1620, 1995.

[19] A.D. Bykhovski, B.L. Gelmont, and M.S. Shur, "Elastic strain relaxation in GaN-AlN-GaN semiconductor-insulator-semiconductor structures," *J. Appl. Phys.*, vol. 78, pp. 3691-3696, 1995.

[20] A.D. Bykhovski, V.V. Kaminski, M.S. Shur, Q.C. Chen, and M.A. Khan, "Piezoresistive effect in wurtzite *n*-type GaN," *Appl. Phys. Lett.*, vol. 68, pp. 818-819, 1996.

[21] P.M. Asbeck, G.J. Sullivan, E.T. Yu, S.S. Lau, and B. McDermott, "Role of the Piezoelectric Effect in AlGaN/GaN HFET Behavior," presented at 55th Device Research Conference (late news), Fort Collins, Colorado, pp. Late News, 1997.

[22] E.T. Yu, G.J. Sullivan, P.M. Asbeck, C.D. Wang, D. Qiao, and S.S. Lau, "Measurement of piezoelectrically induced charge in GaN/AlGaN heterostructure field-effect transistors," *Appl. Phys. Lett.*, vol. 71, pp. 2794-2796, 1997.

[23] R. Gaska, J.W. Yang, A. Osinsky, A.D. Bykhovski, and M.S. Shur, "Piezoeffect and gate current in AlGaN/GaN high electron mobility transistors," *Appl. Phys. Lett.*, vol. 71, pp. 3673-3675, 1997.

[24] P.M. Asbeck, E.T. Yu, S.S. Lau, G.J. Sullivan, J.V. Hove, and J. Redwing, "Piezoelectric charge densities in AlGaN/GaN HFETs," *Electron. Lett.*, vol. 33, pp. 1230-1231, 1997.

[25] R. Gaska, J.W. Yang, A.D. Bykhovski, M.S. Shur, V.V. Kaminski, and S.M. Soloviov, "The influence of the deformation on the two-dimensional electron gas density in GaN—AlGaN heterostructures," *Appl. Phys. Lett.*, vol. 72, pp. 64-66, 1998.

[26] E.T. Yu, P.M. Asbeck, S.S. Lau, and G.J. Sullivan, "Piezoelectric Effects in AlGaN/GaN Heterostructure Field-Effect Transistors," presented at SOTAPOCS, 1998.

[27] L. Hsu and W. Walukiewicz, "Effects of piezoelectric field on defect formation, charge transfer, and electron transport at GaN/$Al_XGa_{1-X}N$ interfaces," *Appl. Phys. Lett.*, vol. 73, pp. 339-341, 1998.

[28] A.D. Bykhovski, R. Gaska, and M.S. Shur, "Piezoelectric doping and elastic strain relaxation in AlGaN—GaN heterostructure field effect transistors," *Appl. Phys. Lett.*, vol. 73, pp. 3577-3579, 1998.

[29] Y.F. Wu, B.P. Keller, S. Keller, D. Kapolnek, P. Kozodoy, S.P. Denbaars, and U.K. Mishra, "Very high breakdown voltage and large transconductance realized on GaN heterojunction field effect transistors," *Appl. Phys. Lett.*, vol. 69, pp. 1438-1440, 1996.

[30] J.P. Ibbetson, K.D. Ness, S.P. DenBaars, U.K. Mishra, P.T. Fini, and J.S. Speck, "Polarization effects, surface states, and the source of electrons in AlGaN/GaN heterostructure field effect transistors," *submitted to Appl. Phys. Lett.*, 1999.

[31] E.T. Yu, X.Z. Dang, L.S. Yu, D. Qiao, P.M. Asbeck, S.S. Lau, G.J. Sullivan, K.S. Boutros, and J.M. Redwing, "Piezoelectric enhancement of Schottky barrier heights in GaN/AlGaN HFET structures," presented at 56th Device Research Conference Digest, Charlottesville, VA, pp.116-117, 1998.

[32] E.T. Yu, X.Z. Dang, L.S. Yu, D. Qiao, P.M. Asbeck, S.S. Lau, G.J. Sullivan, K.S. Boutros, and J.M. Redwing, "Schottky barrier engineering in III-V nitrides via the piezoelectric effect," *Appl. Phys. Lett.*, vol. 73, pp. 1880-1882, 1998.

[33] J. Wang, K.W. Kim, and M.A. Littlejohn, "Carrier capture in pseudomorphically strained wurtzite GaN quantum-well lasers," *Appl. Phys. Lett.*, vol. 71, pp. 820-822, 1997.

[34] T. Wang, D. Nakagawa, J. Wang, T. Sugahara, and S. Sakai, "Photoluminiscence investigation of InGaN/GaN single quantum well and multiple quantum wells," *Appl. Phys. Lett.*, vol. 73, pp. 3571-3573, 1998.

[35] J. Wang, J.B. Jeon, Y.M. Sirenko, and K.W. Kim, "Piezoelectric Effect on Optical Properties of Pseudomorphically Strained Wurtzite GaN Quantum Wells," *IEEE Photon. Tech. Letters*, vol. 9, pp. 728-730, 1997.

[36] T. Takeuchi, C. Wetzel, S. Yamaguchi, H. Sakai, H. Amano, I. Akasaki, Y. Kaneko, S. Nakagawa, Y. Yamaoka, and N. Yamada, "Determination of piezoelectric fields in strained GaInN quantum wells using the quantum-confined Stark effect," *Appl. Phys. Lett.*, vol. 73, pp. 1691-1693, 1998.

[37] S.F. Chichibu, A.C. Abare, M.S. Minsky, S. Keller, S.B. Fleischer, J.E. Bowers, E. Hu, U.K. Mishra, L.A. Coldren, S.P. DenBaars, and T. Sota, "Effective band gap inhomogeneity and piezoelectric field in InGaN/GaN multiquantum well structures," *Appl. Phys. Lett.*, vol. 73, pp. 2006-2008, 1998.

[38] H.S. Kim, J.Y. Lin, H.X. Jiang, W.W. Chow, A. Botchkarev, and H. Morkoç, "Piezoelectric effects on the optical properties of GaN/$Al_xGa_{1-x}N$ multiple quantum wells," *Appl. Phys. Lett.*, vol. 73, pp. 3426-3428, 1998.

[39] H. Kollmer, J.S. Im, S. Heppel, J. Off, F. Scholz, and A. Hangleiter, "Intra- and interwell transistions in GaInN/GaN multiple quantum wells with built-in piezoelectric fields," *Appl. Phys. Lett.*, vol. 74, pp. 82-84, 1999.

[40] L.-H. Peng, C.-W. Chuang, and L.-H. Lou, "Piezoelectric effects in the optical properties of strained InGaN quantum wells," *Appl. Phys. Lett.*, vol. 74, pp. 795-797, 1999.

[41] C. Wetzel, S. Nitta, T. Takeuchi, S. Yamaauchi, H. Amano, and I. Akasaki, "On the bandstructure in GaInN/GaN heterostructures-strain, band gap and piezoelectric effect," *MRS Internet Journal of Nitride Semiconductor Research*, vol. 3, pp. 1-16, 1998.

[42] C. Wetzel, T. Takeuchi, H. Amano, and I. Akasaki, "Piezoelectric Stark-like Ladder in GaN/GaInN/GaN Heterostructures," *Jpn. J. App. Phys.*, vol. 38, pp. L163-L165, 1999.

[43] F. Della Sala, A. Di Carlo, P. Lugli, F. Bernardini, V. Fiorentini, R. Scholz, and J.-M. Jancu, "Free-carrier screening of polarization fields in wurtzite GaN/InGaN laser structures," *Appl. Phys. Lett.*, vol. 74, pp. 2002-2204, 1999.

[44] O. Ambacher, "Growth and applications of Group III-nitrides," *J. Phys. D: Appl. Phys.*, vol. 31, pp. 2653-2710, 1998.

[45] I. Akasaki and H. Amano, "MOVPE Growth of High Quality $Al_xGa_{1-x}N/Ga_yIn_{1-y}N$ ($x>=0$, $y<=1$) Heterostructures for Short Wavelength Light Emitter," *Mat. Res. Soc. Symp.*, vol. 339, pp. 443-452, 1994.

[46] T. Takeuchi, H. Takeuchi, S. Sota, H. Sakai, H. Amano, and I. Akasaki, "Optical properties of strained AlGaN and GaInN on GaN," *Jpn. J. Appl. Phys.*, vol. 36, pp. L177-179, 1997.

[47] H. Ye, G.W. Wicks, and P.M. Fauchet, "Hot electron relaxation time in GaN," *Appl. Phys. Lett.*, vol. 74, pp. 711-713, 1999.

[48] B.R. Chalamala, R.M. Wallace, and B.E. Gnade, "Surface conditioning of active molybdenum field emission cathode arrays with H_2 and helium," *J. Vac. Sci. Technol. B*, vol. 16, pp. 2855-2858, 1998.

[49] B.R. Chalamala, R.M. Wallace, and B.E. Gnade, "Poisoning of Spindt-type molybdenum field emitter arrays by CO_2," *J. Vac. Sci. Technol. B*, vol. 16, pp. 2866-2870, 1998.

[50] B.R. Chalamala, R.M. Wallace, and B.E. Gnade, "Effect of O_2 on the electron emission characteristics of active molybdenum field emission cathode arrays," *J. Vac. Sci. Technol. B*, vol. 16, pp. 2859-2865, 1998.

[51] R. Gomer, *Field Emission and Field Ionization*. Cambridge: Harvard University Press, 1961.

(5) Technology Transfer

- None at this time.